FACULTY OF ELECTRICAL ENGINEERING
KTE
September 7. - 9.9.2009
Cheb, Czech Republic

FAST NUMERIC CALCULATION OF MASSIVE CONDUCTOR 3D MAGNETIC FIELD

PROF. RNDR. ING. MILOSLAV KOŠEK, CSC.
ING. MARTIN TRUHLÁŘ
PROF. ING. ALEŠ RICHTER, CSC.

Abstract: *Preliminary results, theoretical and experimental, dealing with magnetic field in high current three phase net are presented. The simple formula was derived for magnetic field of thin conductor of finite length. According to the formula the flux density decreases at long distance by the second power of distance. The formula makes possible fast numerical calculation of the 3D magnetic field of massive conductors in three phase net. Then the animation of the field flux density is not a problem. The agreement with preliminary experiment is satisfactory, if we take into account a relatively low accuracy of the preliminary experiment. The simple model can be extended by skin-effect and eddy currents effects to be more realistic and allow the estimation of the force between conductors, for instance.*

Key words: *Biot-Savart Law, finite length conductor, dynamic magnetic field, numerical integration, three phase animation, power net conductors*

INTRODUCTION

Big forces can be observed between conductors of high power net, especially in the three phase systems. Also a high temperature increase of some conductors takes a place. The problem is very important; especially from the practical point of view.

We have not made any systematic literature search, but we do not know a work that deals with the problem in detail. It is somewhat surprising for us. Therefore we decided to study the problem systematically [1]. The study is based both on the reliable experiment and careful simulation.

The force acting between conductors is difficult to measure. Since the magnetic field is responsible for the force, the study started with description and measurement of this field. Strictly speaking, as the first step was the description the current distribution in massive conductors due to the skin effect [2, 3].

In order to simulate magnetic field as exact as possible, simple, correct and fast method of calculation is necessary. Usually the finite element method (FEM) is used. In practical case the geometry is simple enough and the application of Biot-Savart Law with numerical integration can be used efficiently. The numerical integration is relatively simple, but time consuming especially in the case, when massive 3D conductor is used and 3D field visualization is necessary. Therefore, simplifications are necessary in order to increase the speed of calculations.

The natural approach is to increase the effectiveness of the algorithm. But the speed increases only a little, usually. Furthermore, there are severe limitations. Another well-known solution is the use of approximations. But the approximations must be used with care; otherwise unexpected results can be obtained. The optimum approach is to use analytical formula that replaces a part of numerical integration and considerably saves computing time. This approach was used in this paper.

1 THEORY

The formula for magnetic field produced by a thin infinite conductor appears in every textbook [4, 5]. The flux density of infinite thin and infinite long conductor is given by the well-known formula

$$B = \frac{\mu_0}{2\pi} I \frac{1}{r}. \qquad (1)$$

where I is current flowing in the conductor, r is the distance from is and μ_o is permeability of vacuum.

However the formula for a thin conductor of finite length can be found in very specialized monographs only.

Because of its key meaning in this paper we present its geometrical deviation in detail here. Another, very brief derivation is in Ref. [6], for instance.

The general geometry is sketched in Fig. 1. Current I flows through the conductor of general shape. Then the contribution of the element $\overrightarrow{dr_0}$ to the flux density is given by the Biot-savart Law in differential form

$$\mathrm{d}\vec{B}(\vec{r}) = \frac{\mu_0}{4\pi} I \frac{\mathrm{d}\vec{r}_0 \times (\vec{r} - \vec{r}_0)}{|\vec{r} - \vec{r}_0|^3} . \qquad (2)$$

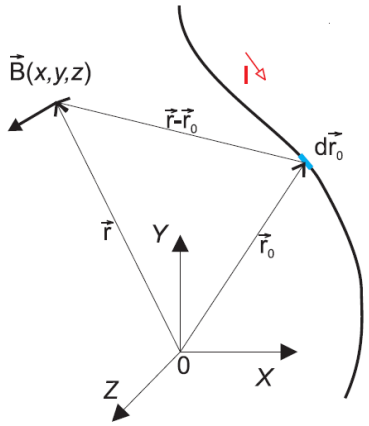

Fig. 1. Biot-Savart Law.

In equation (2) two types of geometrical quantities are used. Position vector with index 0, as $\vec{r}_0 = (x_0, y_0, z_0)$, for instance, defines position of "material" parameters. Material objects are ones that generate magnetic field; in our case the vector $\overrightarrow{ro}$ describes the position of conductor element $\mathrm{d}\vec{r}_0$ with flowing current I, Fig. 1. It is an elementary source of magnetic field. Vectors with no index are used for points where the field is calculated. They are termed field vectors. In equation (2) the field vector is $\vec{r} = (x, y, z)$, for instance, see also Fig. 1.

Equation (2) can be written in more illustrative coordinate form as

$$\begin{aligned}
\mathrm{d}B_x &= \frac{\mu_0}{4\pi} I \frac{\mathrm{d}y_0 (z - z_0) - \mathrm{d}z_0 (y - y_0)}{\sqrt{((x - x_0)^2 + (y - y_0)^2 + (z - z_0)^2)^3}} , \\
\mathrm{d}B_y &= \frac{\mu_0}{4\pi} I \frac{\mathrm{d}z_0 (x - x_0) - \mathrm{d}x_0 (z - z_0)}{\sqrt{((x - x_0)^2 + (y - y_0)^2 + (z - z_0)^2)^3}} , \\
\mathrm{d}B_z &= \frac{\mu_0}{4\pi} I \frac{\mathrm{d}x_0 (y - y_0) - \mathrm{d}y_0 (x - x_0)}{\sqrt{((x - x_0)^2 + (y - y_0)^2 + (z - z_0)^2)^3}} .
\end{aligned} \qquad (3)$$

Now we consider special case, a straight wire of length $2a$ with current I that flows in positive direction of the Z axis[1]. The task is to calculate the flux density **B** in any point. With respect to cylindrical symmetry we consider only a plane that contains the Z axis. The situation is sketched in Fig. 2.

Since the very thin conductor leis in the Z axis, the material vectors and coordinates have the form

$$\vec{r}_0 = (0,0,z_0) \quad \mathrm{d}\vec{r}_0 = (0,0,\mathrm{d}z_0) . \qquad (4)$$

For this case the complete set of equations (3) reduces to simplified form

$$\begin{aligned}
dB_x &= \frac{\mu_0}{4\pi} yI \frac{-dz_0}{\sqrt{x^2+y^2+z^2}^3} , \\
dB_y &= \frac{\mu_0}{4\pi} xI \frac{dz_0}{\sqrt{x^2+y^2+(z-z_0)^2}^3} , \\
dB_z &= 0 .
\end{aligned} \qquad (5)$$

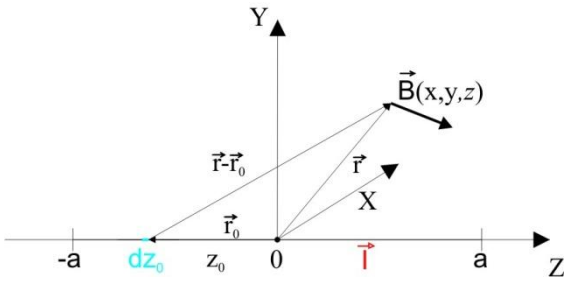

Fig. 2. Biot-Savart Law for wire of finite length

All the important properties of the flux density can be found if we further limit to plane YZ only. In this case $x = 0$ and only equation for x component of flux density remains. In the integral form, it must be written as

$$B_x(y,z) = -\frac{\mu_0}{4\pi} yI \int_{-a}^{a} \frac{dz_0}{\sqrt{y^2+(z-z_0)^2}^3} . \qquad (6)$$

The geometry is sketched in Fig. 3. The flux density in the point with coordinates (y, z) has the only one component $B_x(y, z)$ normal to plane XZ, The x component of flux density has negative sign, since it is oriented in the direction of negative X axis.

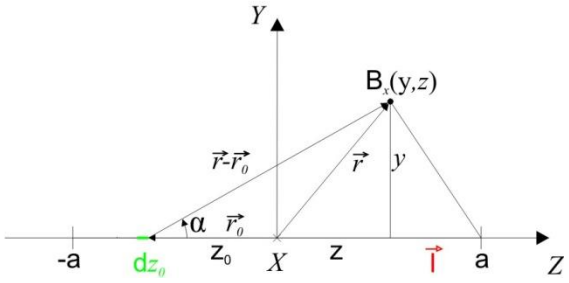

Fig. 3. Geometry in YZ plane used for formula derivation

[1] We ignore the fact that such an arrangement cannot be realized experimentally.

Fig. 3 is well suited for geometrical derivation of analytical formula. The integration for material coordinate z_o will be substituted into integration over material angle α.

Goniometric functions are used for the substitution between differentials $\mathrm{d}z_0$ and $\mathrm{d}\alpha$. Following formulae follows from Fig. 3

$$\operatorname{tg}\alpha = \frac{y}{z - z_0}\,, \qquad (7)$$

$$\sin\alpha = \frac{y}{\sqrt{y^2 + (z - z_0)^2}}\,. \qquad (8)$$

From last equation (8) we found for integrated function the relation

$$\frac{y}{\sqrt{y^2+(z-z_0)^2}^3} = \frac{\sin^3\alpha}{y^2}\,. \qquad (9)$$

From formula (7) we find the relation between old material coordinate z_o and a new variable, angle α.

$$z_0 = z - y\cot\alpha\,. \qquad (10)$$

By differentiating this formula we get relation between differentials $\mathrm{d}z_0$ and $\mathrm{d}\alpha$

$$\mathrm{d}z_0 = y\frac{1}{\sin^2\alpha}\mathrm{d}\alpha\,, \qquad (11)$$

since field coordinates z a y is constant.

After substitution of (11) and (9) into (6) we get very simple formula

$$B_x = \frac{\mu_0}{4\pi}\frac{I}{y}\int_{\alpha_1}^{\alpha_2}\sin\alpha\,\mathrm{d}\alpha = \frac{\mu_0}{4\pi}\frac{I}{y}\,(\cos\alpha_1 - \cos\alpha_2), \qquad (12)$$

where angles α_1 and α_2 are explained in Fig. 4. They have simple geometrical meaning. Observer at point

(x, z), where the field is calculated, sees the wire ends under these angles. Both the angles must be oriented either clockwise (as in fig. 4) or counterclockwise.

For numerical calculations the coordinates are preferred. We get them geometry in Fig. 4 this relations

$$\cos\alpha_1 = \cos(\pi - \alpha') = -\cos\alpha' = -\frac{z''}{\sqrt{y^2+z''^2}} = \frac{a+z}{\sqrt{y^2+(a+z)^2}} \qquad (13)$$

$$\cos\alpha_2 = \frac{z'}{\sqrt{y^2+z'^2}}\frac{a-z}{\sqrt{y^2+(a-z)^2}}$$

Final equation has, after substitution from (13) to (12) this form

$$B_x(\mathrm{y},\mathrm{z}) = \frac{\mu_0}{4\pi}\frac{I}{y}\left[\frac{a-z}{\sqrt{(a-z)^2+y^2}} + \frac{a+z}{\sqrt{(a+z)^2+y^2}}\right]. \qquad (14)$$

Analogical equation can be derived for $B_y(x, z)$ component in plane *XZ*.

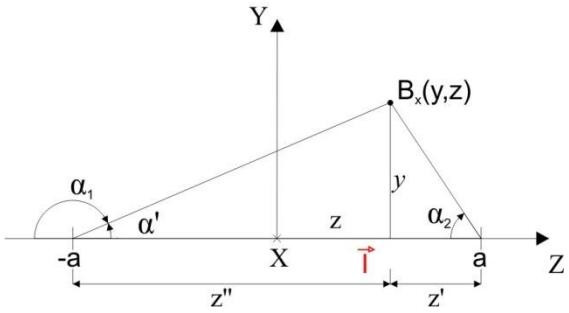

Fig. 4. Limits of integration.

$$B_y(x,z) = \frac{\mu_0}{4\pi}\frac{I}{x}(\cos\alpha_2 - \cos\alpha_1) = = \frac{\mu_0}{4\pi}\frac{I}{x}\left[\frac{a-z}{\sqrt{(a-z)^2+x^2}} + \frac{a+z}{\sqrt{(a+z)^2+x^2}}\right]. \qquad (15)$$

In the case of general oriented plane going thru Z axis the formulae are a little complicated. Both the components exist according to eq. (5). They are functions of all three coordinates, $B_x = B_x(x, y, z)$ $B_y = B_x(x, y, z)$. They are sketched in Fig. 5. The components are given by equations

$$B_x(x,y,z) = -B(x,y,z)\sin\beta = -B\frac{y^2}{\sqrt{x^2+y^2}},$$
$$B_y(x,y,z) = B(x,y,z)\sin\beta = B\frac{x^2}{\sqrt{x^2+y^2}}\,, \qquad (16)$$

where

$$B(x,y,z) = \frac{\mu_0}{4\pi}\frac{I}{\sqrt{x^2+y^2}} \left[\frac{a-z}{\sqrt{x^2+y^2+(a-z)^2}} + \frac{a+z}{\sqrt{x^2+y^2+(a+z)^2}}\right]. \qquad (17)$$

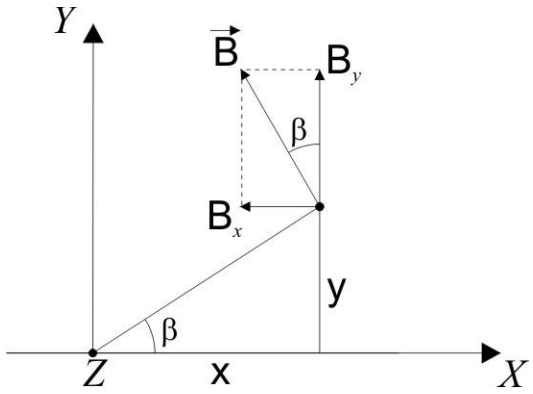

Fig. 5. General form of the flux density.

The final formulae (14) to (17) can be verified in limiting cases. We present it for formula (14). For the field very close to the conductor we can put zero *y*

coordinate, $y = 0$. Then formula (14) changes to (1), if we get $y = r$. The flux density decreases to the first power of distance in agreement with equation (1). In the case of very large distance from conductor we take variable y into the front of both square roots. Then expression $1/y^2$ is in the front o square bracket and the limit of expression in square brackets is zero for y growing to infinity. The flux density decreases to the second power of distance according to equation (2). It the length $2a$ of the conductor increases to infinity we again obtain equation (1).

In the case of straight massive conductor the principle of superposition applies this formula to elementary currents in its cross section. This fact removes summation cycle along the conductor length in numeric integration.

The temperature effect description consists of two stages: transition state after switching the current and steady state for a sufficiently long time after the switching. The steady state is more important. Its physical formulation is relatively simple. The law of energy conservation requires the heat formed in conductors to be transferred into surrounding air. The conductor temperature can be calculated from this physical requirement. No derivation is given here, since the conductor temperature was not studied in detail at present time.

2 EXPERIMENT

Typical applications of research are distribution points. We used simplest way of experimental model of such a three phase distribution point that consists of three massive conductors of rectangular cross-section. Their dimensions are in Fig. 6 and the photograph of experimental setup is in Fig. 7.

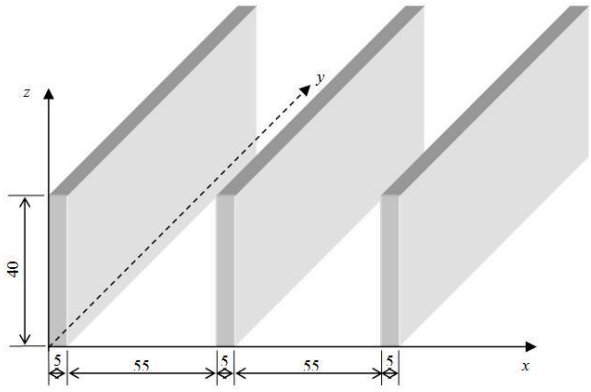

Fig. 6. Geometry of conductors in the experimental model of distribution point.

All the conductors are short-circuited one another as it is seen clearly in Fig. 7. The power net voltage 230/400 V is transformed by three phase transformer to acceptable and adjustable low value voltage for low resistance conductors. Transformer primary is star connected, while the secondary can be switched to star or delta connection.

Fig. 7. Detail of distribution point model realization.

Only the effective current was measured by a clip-on ammeter of a maximum range of 1000 A. The measured currents were 750 A, 914 A and 840 A, respectively, from left to right in Fig. 6. The secondary net is non-symmetric as for current amplitudes. The possible additional shift between phases was not measured at present time.

The magnetic flux density was measured by two means. The hand measurement using commercial instrument was made in the direction of X axis in the centre of conductors very close to their upper end. Only the y component of flux density was measured with relatively low accuracy, Fig. 6.

Most of measurements were semi-automated, however. In order to achieve precise 2D magnetic field measurements, we have realized the positioning system of Hall probe for its location in horizontal line. Vertical position is actually shifted manually. For accurate horizontal position the linear positioning system from old printer driven by step motor was used. The photograph of the apparatus is in Fig. 8. In horizontal line the measurement is fully automated and controlled by the computer. Detailed description is similar to that given in another paper of these proceedings [7].

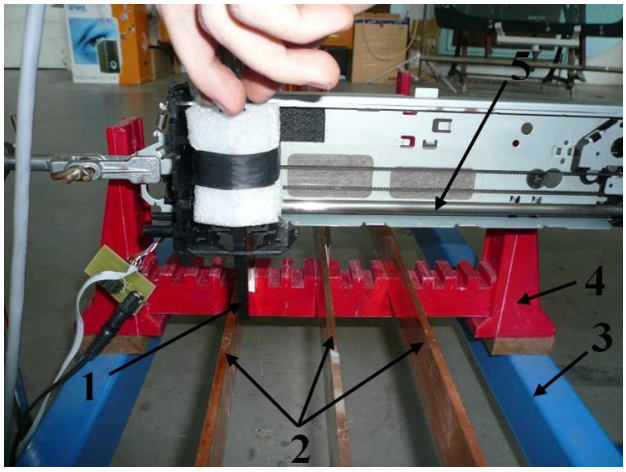

Fig. 8. Apparatus for semi-automated measurement. 1 – 3D Hall probe, 2 – Conductors, 3 – Subrak, 4 – Conductor fixing, 5 – Linear shift

For completeness the block scheme of realized measuring apparatus is shown at Fig. 9. The concept of such a system can be divided to several parts, mechanical part, electronic and measurement part and a control one. Details are in Ref. [7].

Since conductors are driven from three phase net of 50 Hz, the magnetic field change in time. In principle, there are two possibilities: static of dynamic measurement. In static measurement we measure at given point the mean absolute value or the effective one. In dynamic measurement we measure the instantaneous values during the period. Practically sampled values can be scanned.

We preferred dynamic measurements. The total samples per period were 256. This approach requires synchronization of the staring time moment with respect to selected phase. Otherwise, the synchronization can be made from extreme values of data, since in every case one period is scanned. We selected the second approach that is simpler. However, this solution is more complicated and of a low accuracy.

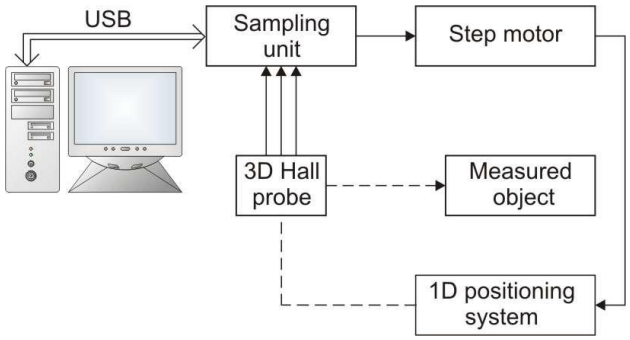

Fig. 9. Block scheme of apparatus control.

Additionally we made preliminary measurement of conductor temperature. Infrared contactless commercial camera was used. The main problem is the emissivity of cooper conductors. Since blank wires are used, their emissivity is low and difficult to estimate. Therefore, the surface of cooper conductors was made black in order to get typical emissivity. Problem was to get uniform value of emissivity. Typical result of temperature scanning is in Fig. 10. The high temperature of central conductor with respect to side ones is surprising.

3 Calculation and Visualization

The calculations of the magnetic field of massive conductors shown in Fig. 6 were made by the use of final equations (14) to (17) of the part Theory. MATLAB was used for calculations, since it appears as an ideal language for technical computing. The base of calculation is to transfer the integrals into numerical summation of small increments.

The first step was to make numerical integration using the general formula (2) which requires 3D integration, over the wire volume. Then the 2D integration was made over the wire cross-section using general formula (16) and (17). The agreement of both results was checked. It was found the results were practically the same if the integration grid was sufficiently fine.

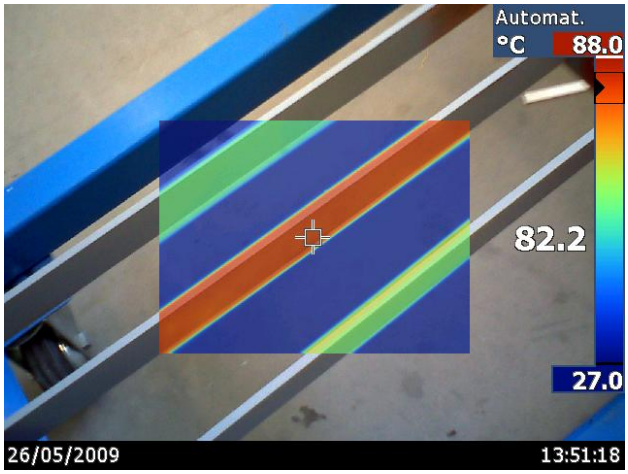

Fig. 10. Temperature distribution in wire.

After this confirmation the filed distribution was calculated in different technical important cuts. For the visualization of results classical parametric graphs were used, since they were found to be the best solution for quantitative information presentation. We tried another means, of course. Surface graphs, 3D imaging, 3D vectors, etc. had low information and illustration value. The only approved method was 2D flux vectors in selected plane. Also the 2D flux lines give interesting results.

4 Results

The investigated conductor has length of 2 m, rectangular cross section with the width of 5 mm and height of 40 mm. DC current of 1000 A was used in all the calculations. It corresponds to the value used in experiments. The coordinate axes used in calculations were the following: *X* axis is in the direction of conductor width, *Y* axis is along conductor height and *Z* axis is the conductor longitudinal axis. The origin is in the centre of conductor.

Results can be presented in three logical areas: typical results of calculation, experimental results and comparison of theory and experiment. The visualization of calculation will be in the form of parametric graphs and flux vectors.

4.1 Parametric graphs

As an example of extensive calculations we present several illustrative examples. The field was calculated in the plane *XZ* or plane parallel to it and in directions either parallel to conductor longitudinal axis or normal to it. Logarithmic scales are often used in order to see details. The most important component is the B_y component in this case. In Fig. 11 there is *y*-component of flux density along lines parallel to conductor longitudinal axis. The parameter is the distance *x* from Z axis. The flux density is normal to the plane *XZ*, therefore the remaining components are of zero value.

It follows from Fig. 11 that near the conductor the field is very uniform almost along all the conductor length. Then the flux density decreases very rapidly. Far

from the conductor (300 mm) the field is not uniform and extends outside the conductor.

The *y* component in basic plane in directions normal to conductor axis and for a high ranges of coordinate *z* is in Fig. 12. For long distances from conductor centre the values initially increase. However, since they are very low, this behavior is only of academic interest.

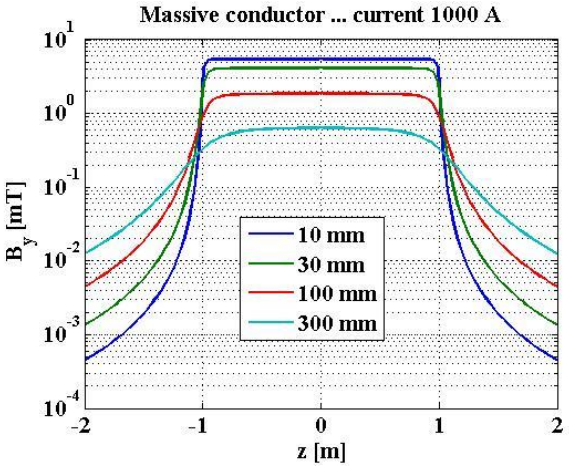

Fig. 11. Flux density parallel to conductor axis in basic plane XZ.

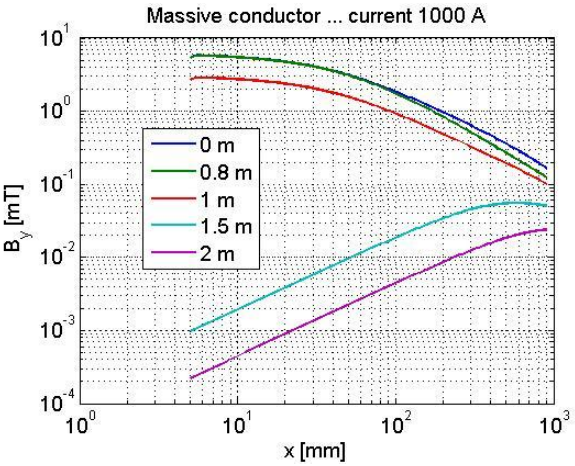

Fig.12: Magnetic field in lines perpendicular to conductor axis and in basic plane XZ.

The components in the direction normal to conductor axis are in Fig 13 and 14 for the plane parallel to plane XZ and in the distance of 24 mm from it, see the parameter in title. It means that the plane is over the conductor and relatively close to it. The parameter in the graph is the distance of the normal lines from conductor centre. In this case both the components of flux density exist and they are shown in the graphs.

The horizontal component B_x achieves high values at the big area near the centre. Near conductor ends its values are close to zero. The negative value is correct, if we consider the orientation of coordinate axes.

The *y* component of flux density according to Fig. 14 changes the sign at plane $x = 0$ in agreement with physical considerations. Analogically to the *x* component its values are also low near conductor ends. In the wide area around the conductor centre this component changes very fast.

Although the calculations are relatively fast, extensive field examination requires a certain time. The question is if the approximations are acceptable. The comparison of fields of infinite and finite length conductors (2 m) are in Fig. 15.

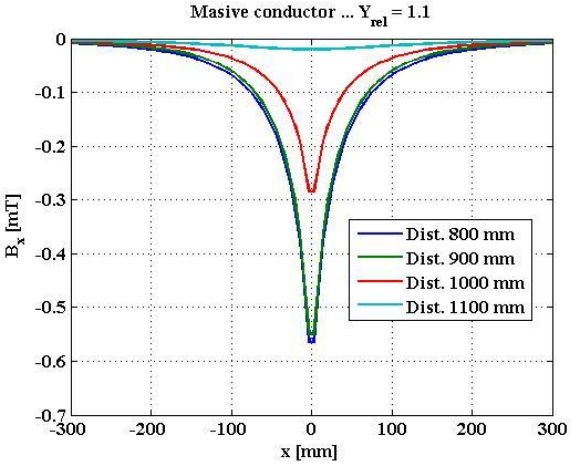

Fig. 13. Component x of flux density normal to conductor axis in plane parallel to basic one XZ.

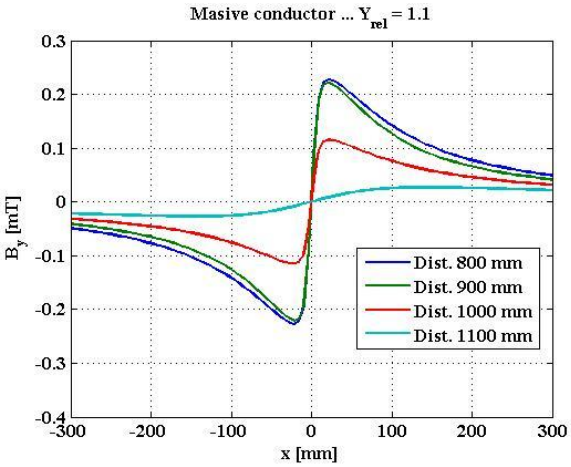

Fig. 14. Component y of flux density normal to conductor axis in plane parallel to basic one XZ.

The distance from conductor centre can be divided into three zones:

1. Near zone, in which the slope of both curves is the same and constant.
2. Middle zone, where the slope of flux density of finite length wire varies.
3. Far zone of constant slope, but of different value from each other.

According to Fig. 15 the middle zone starts very approximately at position $r = 300$ mm and stops at $r = 1000$ mm. Fine scale on *y* axis is necessary for more correct values, but they are not important as we will see later.

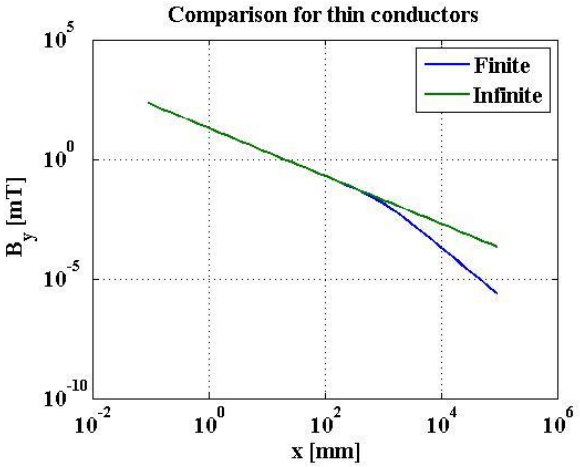

Fig.15: Magnetic field of thin conductors.

For the massive conductor the comparison of numerical calculations and application of approximate formulae is in Fig. 16. The approximation by a finite length thin conductor can be used from distance of about 30 mm. Application of infinite length conductor for approximation is only in narrow range. Again a finer scale for *x* coordinate is necessary to get more precise estimation.

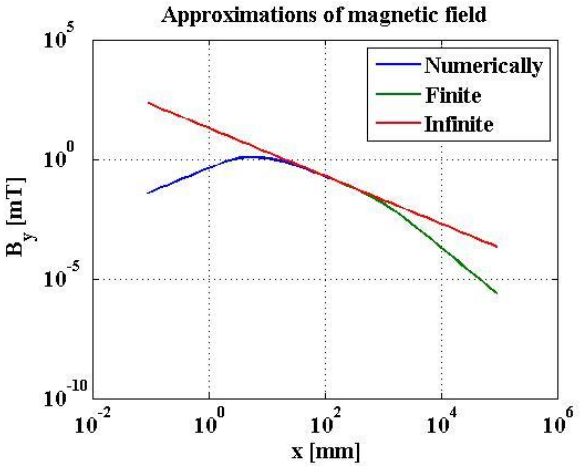

Fig.16: Numeric calculations versus approximations.

4.2 Vector form visualization

Results on Figures above are quantitative, but not illustrative. In order to get a better idea on the field distribution, flux vectors were calculated in planes perpendicular to conductors. A result for a single conductor in its centre is in Fig. 17 and for its end in Fig. 18.

The grid is rectangular in both the Figures and vectors start at its nodes. The illusory deformation is due to the opposite directions of vectors. Only slight difference is between both Figures. It is due to the MATLAB feature. Only the relative changes are visualized. In order to get reliable comparison more complicated approach must be used. These Figures serve as the illustration of the limitation of the method used here. In this case the parametric graphs give correct value and make a simple and correct comparison possible.

The components in parametric graphs in Fig. 11 to 14 are in qualitative agreement with vector form presentation in Fig. 17 or 18. It is enough to make a horizontal line going either through the conductor centre or little above the conductor. The resolution of vector form is low, unfortunately.

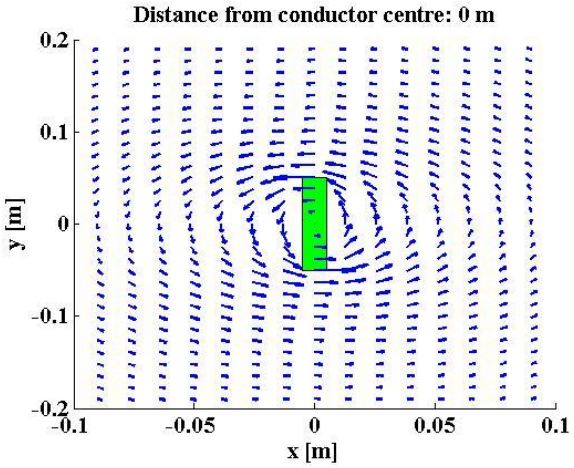

Fig.17: M*agnetic flux vectors in the centre of single conductor.*

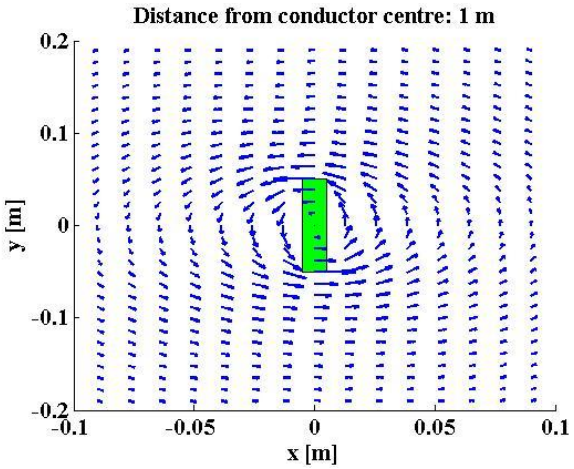

Fig.18: M*agnetic flux vectors at the end of single conductor.*

Dynamical shape of magnetic field in three phase conductors is in Fig. 19 through 22 for important instants of time in a period. The magnetic field is concentrated either in both the gaps between conductors or in the left or right gap. The same is valid for the magnetic energy, which is flowing form one gap to the other.

Only basic features are shown in these Figures. More detailed information can be got from animation that is made for small increase of phase angle of 4^{o}. The rotating magnetic field is almost in whole the area as it is clearly visible in the video. The end point of each vector forms an ellipse. The shape and parameters of the ellipses are quite different depending on their positions.

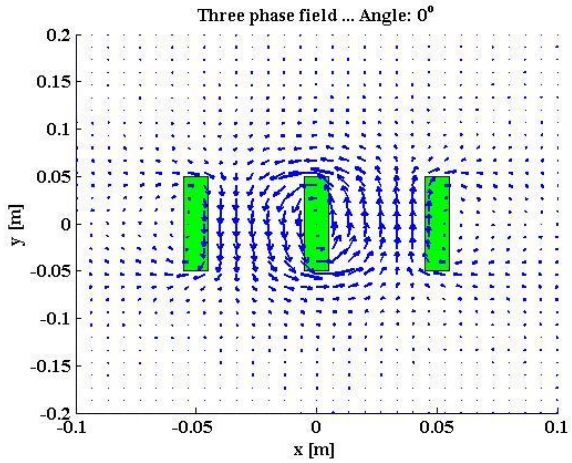

Fig.19: M*agnetic flux vectors for three phase conductors in start of period.*

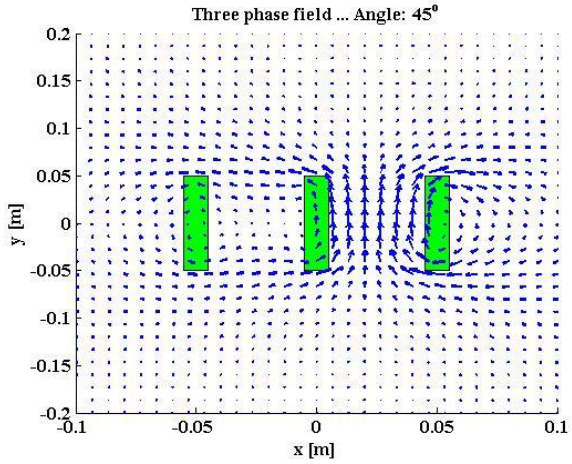

Fig. 20: M*agnetic flux vectors for three phase conductors in one eighth of period.*

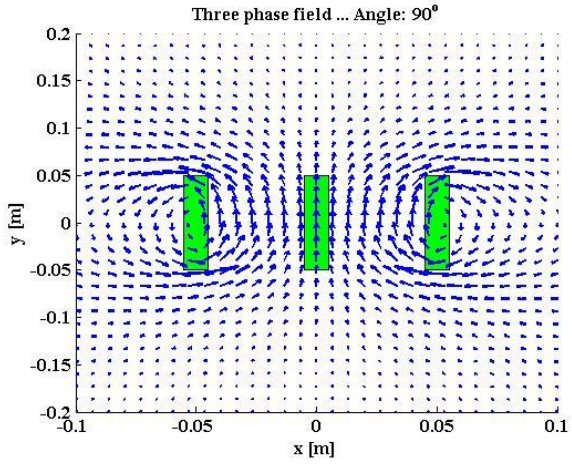

Fig. 21: M*agnetic flux vectors for three phase conductors in one quarter of period.*

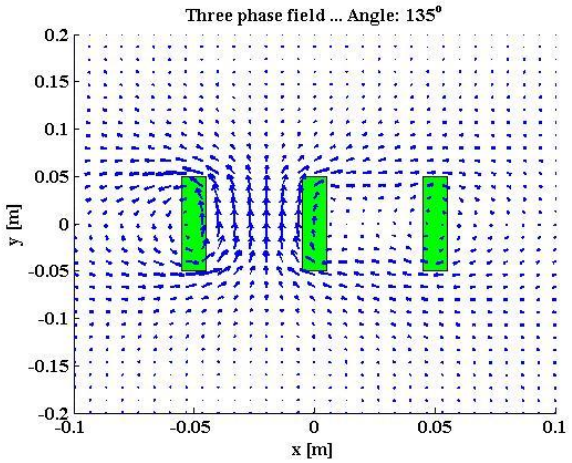

Fig. 22: M*agnetic flux vectors for three phase conductors in three eights of period.*

4.3 Comparison with experiment

First of all, for illustration, two experimental results are presented here. The measurement was made in line very close to upper end of conductors. In Fig. 23 there is a time graph for all three components in the selected relative position near the left hand side of the first conductor. The space shape of all three components of magnetic field short after the start of the period is in Fig. 24. In should be noted that the same coordinate system is used for both the calculations and experimental data processing. The coordinate system sketched in Fig. 6 was used only for direct measurement. Surprisingly high *z* component is in both the Figures. This component should be zero theoretically.

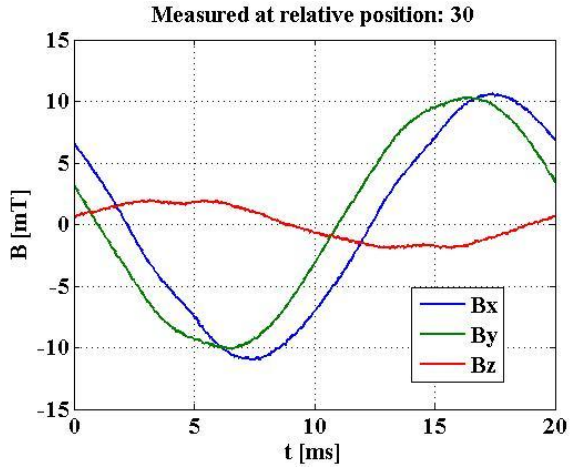

Fig.23: Measured time development of 3D magnetic field during one period.

Comparison between theory and experiment was made in both the time and space domains. The comparison for the time domain is in Fig. 25 for the *x* component of flux density and in Fig. 26 for the *y* component. The agreement is semi quantitative for both the components. The phase shift of about 12^0 is between the experiment and theory for the *x* component of flux

density. There is practically no phase shift for the *y* component. The amplitudes differ significantly. There is no systematic way in the difference. The theoretical value is higher in one case and lower in the second case.

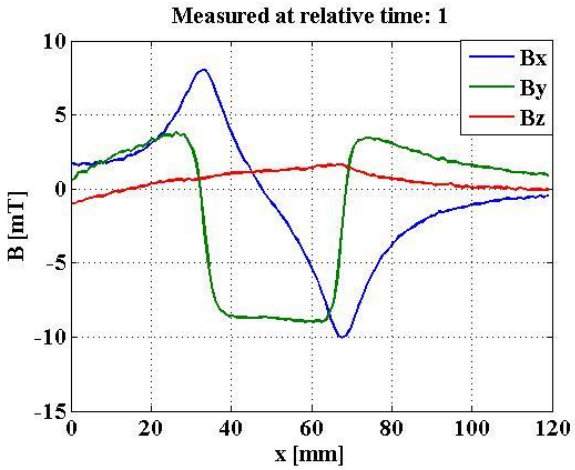

Fig.24: Measured 3D magnetic field on central line at the start of period.

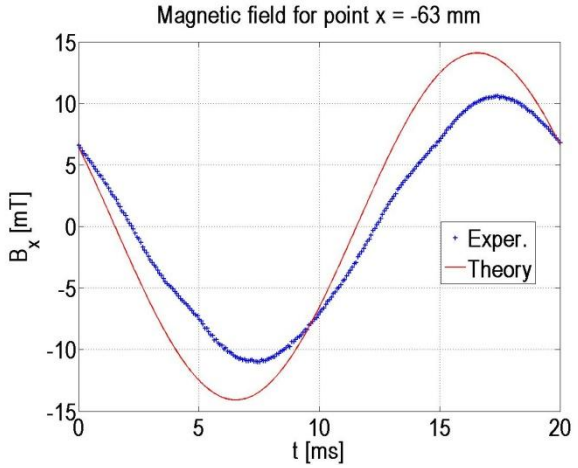

Fig.25: Comparison between theory and experiment in time domain for x component of flux density.

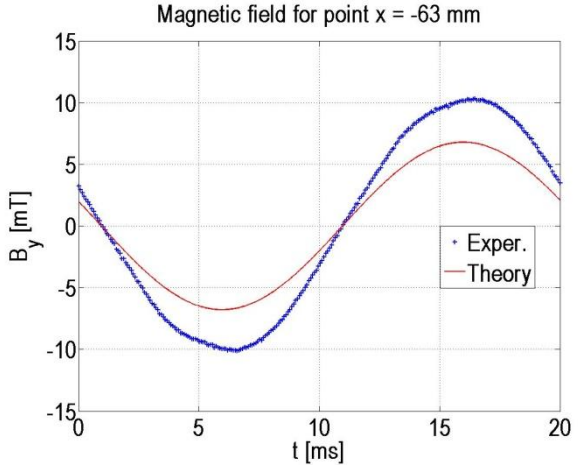

Fig.26: Comparison between theory and experiment in time domain for y component of flux density.

Comparison between theory and experiment in coordinate domain is in Fig. 27 for the *x* component of flux density and in Fig. 28 for the y component. A relative good agreement is in this case, especially for the *y* component.

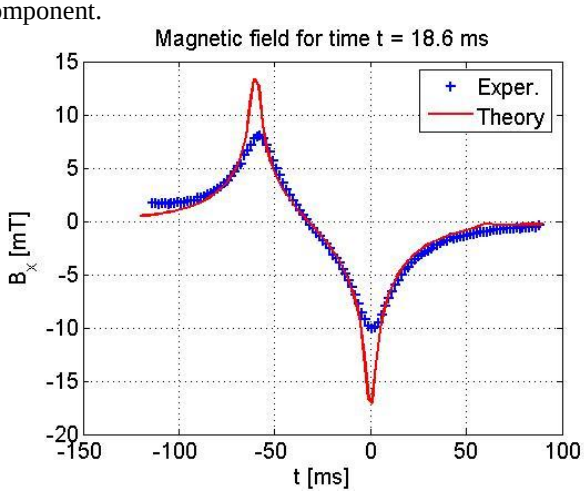

Fig.27: Comparison between theory and experiment in coordinate domain for x component of flux density.

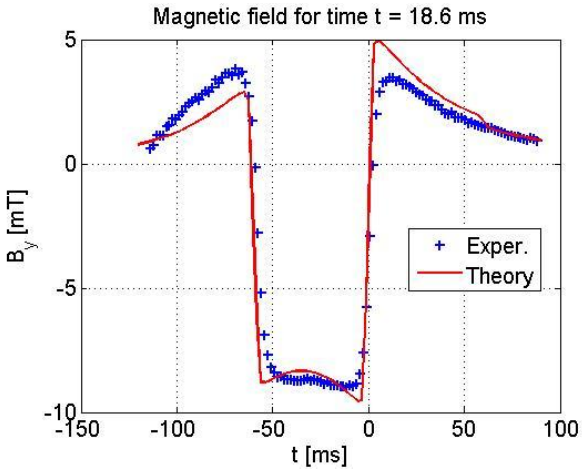

Fig.28: Comparison between theory and experiment in coordinate domain for y component of flux density.

5 DISCUSSION

The application of analytical formula increases the speed of calculations from 50 to more than 1000 times, which allows making animation for three phase field, for instance. The other possibility to increase the speed is approximation. Typical approximations are in Fig. 16. The field of infinite thin conductor decreases with the first power of distance and cannot be used. The field of ideal finite length conductor can be used for far region. It decreases with the second power of distance.

Far region starts approximately at distance of about 30 mm from conductor. However, it is valid only for dimensions of the conductor used in the experiment. If another conductor is used, the far region must be recalculated. Fortunately, it is a very simple procedure.

The agreement with preliminary hand-made experiments that was not given here is satisfactory, if we take into account low probe accuracy and net noise. The main problem is to keep the correct probe angle at hand made measurement. Deviations up to 5^{o} cannot be

recognized. It confirms that the model is suitable and MATLAB scripts are correct.

There is a lot of experimental information for the dynamic case. Only preliminary results were shown. The experimental accuracy is relatively low and it may be the reason of disagreement between theory and experiment is several cases. Main problem is the high value of the *z* component of flux density. At present time we cannot explain this discrepancy.

In the experiment the problem is to measure the field between conductors exactly. Automated measurement in both the directions will be a strong improvement. The control, however, will be difficult in order to avoid probe and conductor collisions.

The results of measured temperature in Fig. 10 are surprising. The relative powers that produce heat in conductors are in Table 1. The power in the central conductor increases by 50 % and in the right hand conductor by 25 %. In Fig. 10 the temperature of central conductor increases considerably, while the temperature of the right hand conductor does not change practically. The temperature change does not correspond to produced heat. More correct temperature measurement and heat transfer modeling will be necessary.

Tab. I. Currents and powers.

Phase	1	2	3
Current [A]	750	914	840
Power ratio	1	1.48	1.25

6 CONCLUSIONS

All the results were achieved by simple numerical method, FEM was not necessary. Possible explanation of differences is the presence of other effects that are not included in the model. Therefore, the further development will be focused to make more realistic models that include the skin-effect and eddy currents at least.

To our knowledge any systematic research of the low voltage distribution net was not made yet. Our preliminary results show that the problem can be treated systematically and correctly. Basic formulae were realized for fast and correct calculations, but they do not include all the effects. The basic models were confirmed by preliminary experiments. Small disagreements that were found could help in the improvement of both the models and experiment technique.

Future work should concentrate to the following subjects mainly:

1. Fully automated experiments.
2. Comparison of calculations with extensive experiments.
3. Study of effect of current non-uniformity in the conductors.
4. Calculation of forces between conductors.
5. Precise measurement of conductor surface temperature.
6. Realization of model that deals with heat effects.

The complex description of the low voltage distribution point will be the goal of future work. Due to the robust and general models this approach can be used simply and efficiently to study the properties of very different realizations or projects of distribution point.

7 ACKNOWLEDGEMENTS

This work was supported by the fund of Ministry of Industry No. FT-TA3/017 and the fund of Czech Science Foundation No. GAČR 102/08/H081.

8 REFERENCES

[1] Truhlář, M, Richter, A.: Skin effect in Busbars of AC Low Voltage (Povrchový jev ve střídavých sběrnicích nízkého napětí), published in EPVE conference proceedings, Czech Republic, Brno 2008, ISBN 978-80-7204-603-4, (in Czech).

[2] Košek, M, Truhlář, M, Richter A.: Detailed and full description of skin effect (Podrobný a úplný popis skinefektu), published in Slaboproudý obzor, Vol. 64, 2008, No. 1-2, pp. 25-28, ISSN 0037-668X (in Czech).

[3] Truhlář, M, Richter, A.: The Skin Effect within Three Phase 50 Hz Power Net with High Current Load, published in ECMS, 9th International Workshop on Electronics, Control, Modelling, Measurement and Signals, July, 8 – 10, 2009, Mondragon, Spain, pp. 197 – 202.

[4] Haňka L. Theory of electromagnetic field, SNTL, Praha, 1975. (in Czech).

[5] Inan U, S, Inan A, S.: Engineering electromagnetics, published in Menlo Park, California, Addison-Wesley, Inc.

[6] Frollo, J., Andris, P., Přibil, J., Vojtíšek, L., Holúbeková, Z., Dremek, T.: Magnetic Field Measurement of a Planar coil using Magnetic resonance Imaging Methods, published in MEASUREMENT 2009, Proceeding of the 7th Interantional Conference on Measurement, Smolenice, Slovakia, May 20 = 23, 2009, pp 258 = 261, ISBN 978-80-969672-1-6.

[7] Mikolanda, T., Košek, M., Richter, A.: 3D Magnetic Field of Permanent Magnets, Simulation and Measurement, published in these proceedings.

Prof. RNDr. Ing. Miloslav Košek, CSc.
Prof. Ing. Aleš Richter, CSc.
Ing. Martin Truhlář
Technical University of Liberec
Studentská 2
461 17 Liberec
Czech Republic

miloslav.kosek@tul.cz
ales.richter@tul.cz
martin.truhlar@tul.cz